Chapter 4
The Chemical Reactivity of Fullerenes and Endohedral Fullerenes: A Theoretical Perspective

Sílvia Osuna[1], Marcel Swart[1,2], and Miquel Solà[1]

Abstract We report here a review of our recent efforts at understanding and predicting reactivity and regioselectivity of endohedral (metallo)fullerenes and their parent free fullerenes. The effect of encapsulation of trimetallic nitrides or noble gas atoms/dimers was shown to have a profound impact on the stability and reactivity of fullerene compounds. It is not just the encapsulation, but in particular the nature of the species that is encapsulated that determines how (un)reactive the fullerene becomes. These findings have important consequences for future applications of (metallo)fullerenes in biomedicine and (nano)technology.

4.1 Introduction

Soon after the discovery of the buckminsterfullerene (C_{60}), it was hypothesized that the diameter of this molecule was large enough to encapsulate a variety of atoms inside the carbon cage (Kroto et al. 1985). Indeed, the first stable metallofullerene based on the "bucky ball" ($La@C_{60}$) was detected in the same year as the initial discovery (Heath et al. 1985), and some years later the formation of higher fullerenes encapsulating a lanthanum atom, such as $La@C_{70}$, $La@C_{74}$, and

[1] Institut de Química Computacional and Departament de Química, Universitat de Girona, Campus Montilivi, 17071 Girona, Catalonia, Spain
e-mail: silvia.osuna@udg.edu; miquel.sola@udg.edu

[2] Institució Catalana de Recerca i Estudis Avançats (ICREA), Pg. Lluís Companys 23, 08010 Barcelona, Spain
e-mail: marcel.swart@udg.edu

M.V. Putz (ed.), *Carbon Bonding and Structures: Advances in Physics and Chemistry*, Carbon Materials: Chemistry and Physics 5, DOI 10.1007/978-94-007-1733-6_4,

La@C_{82} was reported in macroscopic quantities (Chai et al. 1991). It was in the same study, where the symbol @ was introduced to denote that the former atom or molecule is encaged inside the fullerene molecule. These species containing atoms or molecules inside the fullerene cages are called endohedral fullerenes (EFs). The most studied compounds are the so-called endohedral metallofullerenes (EMFs) due to their high abundancy (Akasaka and Nagase 2002). In 1991, the first structural characterization by X-ray diffraction of an EMF was reported (Chai et al. 1991).

EMFs can be classified in several classes (Chaur et al. 2009): (i) classical EFs of the type M@C_{2n} and M_2@C_{2n} (M = *metal, noble gas, small molecule and* $60 \leq 2n \leq 88$); (ii) trimetallic nitride EMFs ($M_3N@C_{2n}$, M = *metal and* $68 \leq 2n \leq 96$); (iii) metallic carbide EMFs ($M_2C_2@C_{2n}$, $M_3C_2@C_{2n}$, $M_4C_2@C_{2n}$, *and* $M_3CH@C_{2n}$ *with* M = *metal and* $68 \leq 2n \leq 92$); (iv) metallic oxide EMFs ($M_4O_2@C_{2n}$ *and* $M_4O_3@C_{2n}$); and (v) metallic sulfide ($M_2S@C_{2n}$). Of course, as the number of EFs families and the elements of each family increase rapidly this current classification will be modified in the future.

The high interest awakened by these EMFs is in part motivated by the promising potential applications of these compounds in a wide range of research topics such as magnetism, superconductivity, and nonlinear optical (NLO) properties (Whitehouse and Buckingham 1993; Hu et al. 2008). For instance, the opto-electronic properties of EMFs might be tailored without changing the outer carbon cage by changing the metal cluster encapsulated inside the cage. The encapsulation of the metals inside the carbon fullerene cage makes these compounds ideal for medical applications, for example as hosts of radioactive atoms for use in nuclear medicines (Diener et al. 2007; Shultz et al. 2010) or as effective magnetic resonance imaging (MRI) contrast agents (Dunsch and Yang 2007; Laus et al. 2007). In addition, EMFs used as electron acceptor in electron donor–acceptor dyads can lead to promising photovoltaic materials to be used in solar energy conversion/storage systems (Guldi et al. 2010). The use of some EFs with long spin lifetime for quantum computing or spintronic devices has also been suggested (Pietzak et al. 2002; Harneit 2002). Finally, they have also been used for monitoring chemical reactions of the fullerene cages via changes in the electron paramagnetic resonance (EPR) signals (Pietzak et al. 2002; Wang et al. 2001).

The stability and reactivity of the fullerene cages is highly modified after the encapsulation due to the interaction between the inner species and the carbon cage. For instance, the C_{80} cage of I_h symmetry is the most unstable among the seven structures of C_{80} that satisfy the isolated pentagon rule (IPR) (Kroto 1987; Schmalz et al. 1988). However, this is the preferred cage for encapsulating two La atoms or a Sc_3N unit. Indeed, $Sc_3N@I_h$-C_{80} is the third most abundant fullerene after C_{60} and C_{70} (Valencia et al. 2009). Similar situations are found for other fullerene cages such as the D_{3h}-C_{78} and C_{2v}-C_{82}. On the other hand, while the IPR is strictly followed by all pure-carbon fullerenes isolated to date (Lu et al. 2008), an increasing number of EMFs have been synthesized that present non-IPR cages. Therefore, the IPR appears to be more a suggestion than a rule for these species (Kobayashi et al. 1997) and, in general, for any

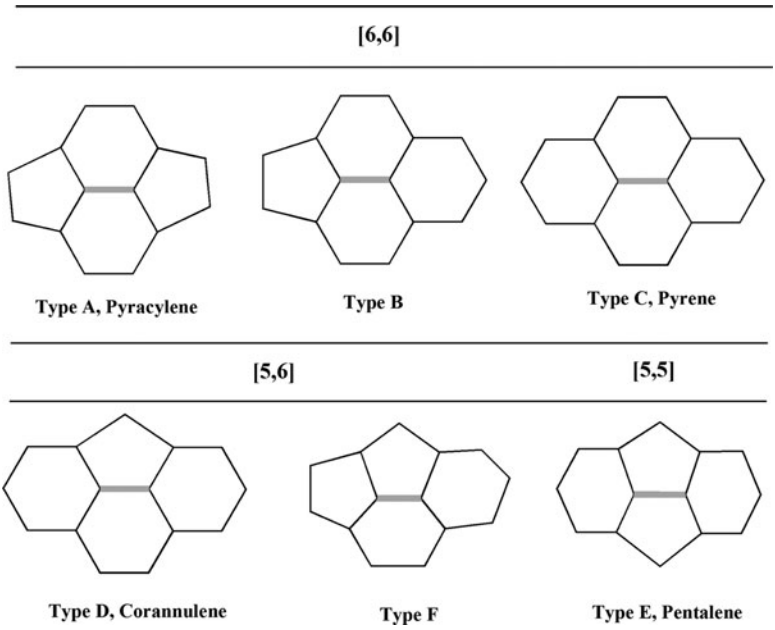

Fig. 4.1 Representation of the different [6,6], [5,6], and [5,5] bond types that may be present in any fullerene structure

charged fullerene (Aihara 2001). In non-IPR carbon cages, there are six possible different C–C bond types A to F (represented in Fig. 4.1), where types E and F are not present in IPR structures.

4.1.1 Trimetallic Nitride Template (TNT) Fullerenes

A rule for the stabilization of fullerene cages in metallic nitride EMFs has been recently established based on the fact that there is a formal charge transfer of six electrons from the nitride to the carbon cage, i.e. $M_3N^{6+}@C_{2n}{}^{6-}$ (Popov and Dunsch 2007, 2009). According to the maximum hardness principle (Pearson 1997, 1999; Parr and Chattaraj 1991; Torrent-Sucarrat et al. 2001), Campanera and coworkers concluded that the most stable metallic nitride EMFs are those encapsulated in fullerene cages that present large (LUMO-4)-(LUMO-3) gaps (Campanera et al. 2005; Valencia et al. 2007).

The metal cluster encapsulated inside the fullerene cages has an enormous influence on the reactivity of these compounds (Guha and Nakamoto 2005; Martín 2006), which is, in general, reduced in TNT EMFs as compared to free fullerenes

(Campanera et al. 2005, 2006; Osuna et al. 2008). Many recent experimental and theoretical studies show that not only the chemical reactivity but also the regioselectivity of TNT EMFs is strongly affected by the encapsulated cluster, metal species, carbon cage size, and symmetry (Akasaka and Nagase 2002; Thilgen and Diederich 2006; Martín 2006; Cardona et al. 2005a; Iiduka et al. 2005).

The production of endohedral compounds such as $Sc_3N@C_{80}$, $Sc_3N@C_{78}$ or $Sc_3N@C_{68}$ in high yields using the so-called trimetallic nitride template (TNT) process, led to the organic functionalization of these fascinating molecules (Stevenson et al. 2000). In 2002, the Diels-Alder reaction was successfully produced for the first time on the I_h isomer of $Sc_3N@C_{80}$ (Lee et al. 2002). The crystallographic characterization of the first Diels-Alder adduct performed on an endohedral metallofullerene indicated that a symmetric adduct was obtained after reaction with 6,7-dimethoxyisochroman-3-one (Lee et al. 2002). The addition was shown to occur on the corannulene-type [5,6] bonds. Campanera et al. performed theoretical calculations (Campanera et al. 2006) that correctly describe the reactive exohedral sites of $Sc_3N@C_{80}$ for the Diels-Alder reaction. Based on these studies, the most reactive sites were those with high Mayer Bond Order (MBO) (Mayer 1983) and high pyramidalization angles (Haddon 2001; Haddon and Chow 1998). The geometry of the Diels-Alder adduct was similar to that found for the reaction on C_{60}, where the usual reactive bonds are the pyracylene-type [6,6] bonds. It should be mentioned here that the I_h isomer of $Sc_3N@C_{80}$ does not possess the reactive pyracylene-type bonds. In 2005, the 1,3-dipolar cycloaddition of N-ethylazomethine ylide and $Sc_3N@C_{80}$ was reported (Cardona et al. 2005b) where the same addition pattern, i.e. over the [5,6] bonds, was produced. In contrast, the 1,3-dipolar cycloaddition involving N-tritylazomethine ylide and $Sc_3N@C_{80}$ led to two different monoadducts. The thermodynamic control product was shown by both NMR and X-ray crystallography to correspond to the [5,6] addition, however the [6,6] adduct was the kinetic control addition product (Cai et al. 2006). Interestingly, the 1,3-dipolar cycloaddition to the parent $Y_3N@C_{80}$ lead to the [6,6] addition (Cardona et al. 2005b). The same regioselectivity was observed in the cyclopropenation reaction of diethyl bromomalonate and $Y_3N@C_{80}$ (Cardona et al. 2005b). The X-ray structure indicated that the C–C bond attacked is open rather than closed and that one of the yttrium atoms is positioned near the site of the cleaved bond. It should be noted here that the carbene addition to $Y@C_{82}$ was shown to yield an open fulleroid [6,6] regioisomer whose attacked bond was situated close to one of the yttrium atoms (Lu et al. 2009). Moreover, the 1,3-dipolar cycloaddition performed on the $M_2@I_h$-C_{80} (M = La, Ce) yielded two regioisomeric adducts corresponding to the [6,6] and [5,6] addition (Yamada et al. 2009). Interestingly, the M_2 cluster is facing the attacked bond in the case of the [5,6] product. The isomerization from the [6,6] to the [5,6] regioisomer was observed in the case of $Y_3N@$(N-Ethylpyrrolidino-C_{80}) (Cardona et al. 2006; Echegoyen et al. 2006). This was also the case for the N-ethylazomethine ylide addition to $Er_3N@C_{80}$ (Cardona et al. 2006). Theoretical calculations at the BP86/TZ2P level for the $Y_3N@$(N-Ethylpyrrolidino-C_{80}) indicated that the

isomerization process takes place through a pirouette-kind of mechanism instead of involving the retro-cycloaddition reaction from the [6,6] adduct (Rodríguez-Fortea et al. 2006). The 1,3-dipolar cycloaddition was also produced to the encapsulated mixed-metal clusters $Sc_2YN@C_{80}$ and $ScY_2N@C_{80}$ (Chen et al. 2007a). As mentioned above, the reaction on $Sc_3N@C_{80}$ and $Y_3N@C_{80}$ was shown to give [5,6] and [6,6] cycloaddition adducts, respectively. Interestingly, the major adduct obtained in the case of the metal mixed Sc_2YN endohedral compound corresponded to the [5,6] addition as it happens with its parent $Sc_3N@C_{80}$. A change on the regioselectivity is produced with the encapsulation of two or more yttrium atoms (i.e. ScY_2N and Y_3N) inside the cage. The [6,6] product is the minor adduct in the case of $ScY_2N@C_{80}$, whereas in $Y_3N@C_{80}$ only the [6,6] regio-isomer is obtained. These findings suggest that the nature of the metal cluster encapsulated inside dictates the exohedral functionalization of the endohedral metallofullerenes.

The Diels-Alder reaction on the D_{5h} isomer of $Sc_3N@C_{80}$ and $Lu_3N@C_{80}$, and 1,3-dipolar cycloadditions to the D_{5h} isomer of $Sc_3N@C_{80}$ indicated a higher reactivity of the D_{5h} isomer as compared to the I_h isomer (Cai et al. 2006). The latter increase on the reactivity was explained in terms of the HOMO-LUMO energy gaps for both isomers (Cai et al. 2006). The LUMO orbitals of the D_{5h} isomers of $Sc_3N@C_{80}$ and $Lu_3N@C_{80}$ are comparable to those of the I_h isomer, whereas a destabilization of the HOMOs for the D_{5h} isomer is produced. The D_{5h} isomer was shown to be 21.1 $kcal{\cdot}mol^{-1}$ less stable at PBE/TZ2P than the corresponding I_h isomer (Popov and Dunsch 2007). Interestingly, the D_{5h} isomer presents the reactive pyracylene-type [6,6] bonds (the most reactive bond in the case of C_{60}). The 1,3-dipolar cycloaddition reaction performed on $Sc_3N@D_{5h}$-C_{80} yielded two possible monoadducts (Cai et al. 2006). The NMR spectrum for the thermodynamically stable cycloadduct was thought to be resulting from reaction at the pyracylene-type [6,6] bond. The other regioisomer obtained corresponding to the addition to an asymmetric bond, presumably of [6,6] type, was partially converted after heat treatment to other unidentified monoadducts.

The Diels-Alder reaction with ortho-quinodimethane and the gadolinium based metallofullerene $Gd_3N@C_{80}$ was achieved in 2005 (Stevenson et al. 2005). The latter compound is of significant interest because of its potential applications as MRI contrast agent (Agnoli et al. 1987). It was shown that two o-quinodimethane molecules were attached to the $Gd_3N@C_{80}$ surface (i.e. the formation of a bisadduct). The yield of the reaction was modest as only 0.5–1 mg of bisadduct was obtained from 5 mg of $Gd_3N@C_{80}$ (10–20%). For comparison, the yield of the 1,3-dipolar reaction on $Sc_3N@C_{80}$ is 30–40% (Cai et al. 2005). A combined theoretical and experimental investigation of the change on the regioselectivity of the 1,3-dipolar cycloaddition and a series of gadolinium and scandium mixed endohedral metallofullerenes ($Sc_xGd_{(3-x)}N@C_{80}$) was performed in 2007 (Chen et al. 2007b). The regioselectivity of the reaction was changed upon introduction of gadolinium atoms. The [5,6] product was the major adduct in $Sc_3N@C_{80}$, $Sc_2GdN@C_{80}$, and $ScGd_2N@C_{80}$, however the [6,6] adduct was also obtained

in $Sc_2GdN@C_{80}$ and $ScGd_2N@C_{80}$. The [6,6] regioisomer was the major cycloaddition product in the case of $Gd_3N@C_{80}$. Interestingly, the thermal treatment of the final products led to the partial or total isomerization of the [6,6] adducts formed in the case of $Sc_2GdN@C_{80}$ and $ScGd_2N@C_{80}$ to the [5,6] regioisomers, respectively. Experimental and theoretical findings showed that the difference in stability between [6,6] and [5,6] products in the case of $ScGd_2N@C_{80}$ is very small (*the [5,6] adduct is at PBE/DNP just 2.3* kcal·mol^{-1} *more stable than the [6,6] one*). This energy difference ranges from 11.7 to −0.4 kcal·mol^{-1} along the series $Sc_3N@C_{80} > Sc_2GdN@C_{80} > ScGd_2N@C_{80} > Gd_3N@C_{80}$. The reactivity of the gadolinium based endohedral compounds $Gd_3N@C_{80}$, $Gd_3N@C_{84}$, and $Gd_3N@C_{88}$ was investigated to study the effect of the cage size on the exohedral reactivity (Chaur et al. 2008). They observed that among all considered compounds $Gd_3N@C_{80}$ was the most reactive cage through reaction with bromomalonate. The flattened shape of C_{84} and C_{88} cages makes them less pyramidalized and thus less reactive upon the Bingel reaction.

The synthesis and characterization of the first N-tritylpyrrolidino derivative of $Sc_3N@C_{78}$ utilizing the Prato reaction was successfully produced in 2007 (Cai et al. 2007). On the basis of NMR spectra and DFT calculations, Cai and coworkers concluded that the two monoadducts obtained corresponded to the addition to two different type B [6,6] bonds (called c-f and b-d). The X-ray diffraction of one of the obtained compounds (c-f addition) confirmed that the 1,3-dipole was attached to a [6,6] bond (Cai et al. 2007). It is interesting to remark here that the cyclopropanation reaction of $Sc_3N@C_{78}$ and diethyl bromomalonate yielded one monoadduct and one dominant symmetric bisadduct, which corresponded to the same type B [6,6] addition (Cai et al. 2008). The photochemical addition reaction of adamantylidene to $La@C_{78}$ was produced on both a [6,6] and a [5,6] bond (Cao et al. 2008).

Tremendous efforts have been devoted to the functionalization of EMFs and to get a better understanding of the reactivity of EMFs. Nevertheless, the development of regioselective reactions for EMFs is still in its infancy. The main reason is the difficulty to produce and isolate sufficient quantities to investigate their reactivity. Although this has been improved over the years (Tellgmann et al. 1996) and now there are companies offering EMFs at affordable prices (see e.g. http://sesres.com), still the low EMF yields limit the investigations on the EMFs reactivity to mainly the most abundant EMFs. Theoretical studies are important to predict or to give support to possible addition sites. In this chapter, studies on the exohedral reactivity of the free cages D_{3h}-C_{78}, C_2-C_{78} and the corresponding TNT EMFs derivatives $X_3N@D_{3h}$-C_{78} (X = Sc, Y) and $X_3N@C_2$-C_{78} (X = Sc, Y) will be discussed. First, the theoretical exploration of the exohedral reactivity of the free cages upon the Diels-Alder reaction with 1,3-cis-butadiene will be explored. Afterwards, the effect of the encapsulation of different TNT units on the regioselectivity and reactivity of the fullerene cage will be presented. Then, the Diels-Alder cycloaddition reaction will be investigated on the preferred isomer of C_{78} for encapsulating large TNT units such as Y_3N. Finally, the effect of the encapsulation of noble gas atoms or dimers on the reactivity of C_{60} will be briefly explored.

4.2 Chemical Reactivity of D_{3h}-C_{78} and Its Endohedral Derivative $Sc_3N@C_{78}$

Although the exohedral reactivity of free fullerenes is quite well-understood, how TNT endohedral metallofullerenes react is still unclear as different factors counteract. An increase of the reactivity might be expected taking into account that the insertion of the TNT unit leads to a higher pyramidalization of some carbon atoms. The more pyramidalized the C–C bond being attacked, the closer it is to the sp^3 bonding situation of the final adduct and the lower the deformation energy of the cage. On the other hand, the electronic transfer produced from the TNT unit to the fullerene reduces the electron affinity of the cage which implies that a reduction of the reactivity might be produced. Moreover, the LUMO orbitals of the endohedral compound are destabilized because of the charge transfer of six electrons from the metal cluster to the fullerene cage, thus disfavoring the interaction with the HOMO of the diene. In contrast to C_{80}, the rotation of the TNT unit encapsulated inside the C_{78} cage is highly impeded (Campanera et al. 2002), and therefore the study of how the reactivity of the different bonds is affected by the metal insertion can be directly investigated. The Diels-Alder [4 + 2] reaction has been studied with the BP86/TZP//BP86/DZP method over the 13 non-equivalent bonds of the D_{3h}-C_{78} and $Sc_3N@D_{3h}$-C_{78} compounds (see Fig. 4.2) (Osuna et al. 2008).

In Fig. 4.2, all non-equivalents bonds are marked in the fullerene compound, as well as the activation barriers obtained for every addition site. D_{3h}-C_{78} has seven non-equivalent [6,6] type bonds that can be classified in three subtypes: (i) pyracylenic of type A (*bonds called **1** and **7**, see Fig.* 4.2), (ii) type B (*bonds **3**, **4**, **5**, and **6***) and (iii) pyrenic of type C (*bond **2***). Furthermore, there are six [5,6]

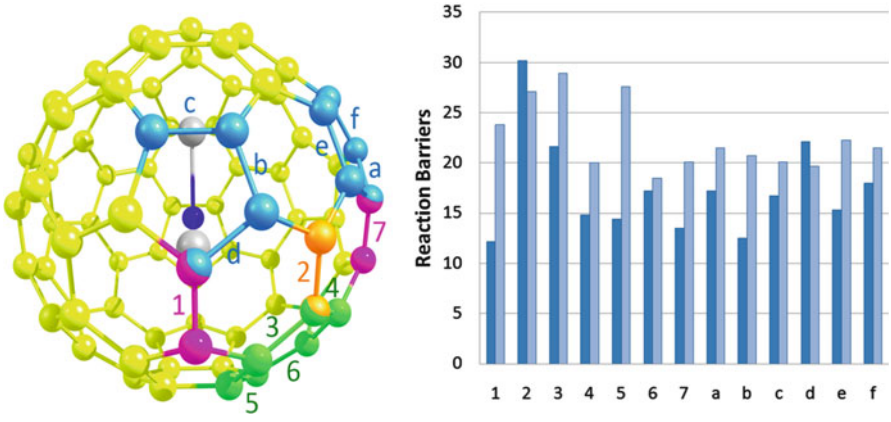

Fig. 4.2 Representation of all non-equivalents bonds of the $Sc_3N@C_{78}$ endohedral fullerene, and the activation barriers obtained for the Diels-Alder reaction on the free C_{78} (*represented in dark blue*) and the $Sc_3N@C_{78}$ (*represented in light blue*) compounds. All energies are represented in kcal·mol^{-1}

type bonds of type D (*corannulene, **a–f***). We will refer to each different bond according to this nomenclature, where for example number **1** is used to denote the pyracylenic or type A bond situated in the position indicated in Fig. 4.2.

The Diels-Alder reaction on the free D_{3h}-C_{78} cage is basically favored over a [5,6] bond called **b** and two type A [6,6] bonds (bonds **1** and **7**) (Osuna et al. 2008). The corannulene (type D) [5,6] bond **b** presents a reaction energy of -23.9 kcal·mol^{-1} and an activation barrier of 12.5 kcal·mol^{-1}. Pyracylenic (type A) bonds called **1** and **7** do also present favorable reaction and activation barriers (for bond **1**: $\Delta E_R = -16.0$ kcal·mol^{-1}, $\Delta E^{\ddagger} = 12.2$ kcal·mol^{-1}, and for bond **7**: $\Delta E_R = -18.8$ kcal·mol^{-1}, $\Delta E^{\ddagger} = 13.5$ kcal·mol^{-1}). It is important to remark here that pyracylene bonds correspond to the most favorable addition sites for C_{60}, which is indeed also the case for the free D_{3h}-C_{78} cage.

The encapsulation of the scandium based metal cluster inside the D_{3h}-C_{78} cage (i.e. $Sc_3N@D_{3h}$-C_{78}) involves a change in the regioselectivity of the reaction. The most reactive bonds are two type B [6,6] bonds called **6** and **4**, and one [5,6] type D bond called **c**. The reaction energies obtained are -12.7, -9.7 and -10.4 kcal·mol^{-1} for the addition over **6**, **4** and **c**, respectively. Furthermore, a huge destabilization is produced after the TNT encapsulation, as most of the considered bonds become less reactive by approximately 12–20 kcal·mol^{-1}. A high destabilization is observed for those bonds situated close to the scandium atoms (especially for **1** and **b**). The only case where the cycloaddition reaction is enhanced after the encapsulation is over bond **6** which is stabilized by ca. 17 kcal·mol^{-1}. Interestingly, the lowest activation barrier is found for bond **6** (18.5 kcal·mol^{-1}), which also presents the most exothermic reaction energy. It should be noted that the most favorable addition site in $Sc_3N@D_{3h}$-C_{78} presents an activation barrier which is 6.3 kcal·mol^{-1} higher in energy than the lowest found for the free cage (18.5 kcal·mol^{-1} for bond **6** in $Sc_3N@D_{3h}$-C_{78} as compared to 12.2 kcal·mol^{-1} for bond **1** in D_{3h}-C_{78}). However, the reaction becomes less regioselective as bonds **4**, **7**, **b**, **c**, and **d** present activation barriers within the range of 19.7–20.7 kcal·mol^{-1}. Interestingly, the 1,3-dipolar cycloaddition reaction on $Sc_3N@D_{3h}$-C_{78} yielded two cycloaddition products corresponding to the addition to the [6,6] bonds called **6** and **4** (Cai et al. 2007). Although our calculations indicate that the reaction might also be favorable over bond **c** (**7** and **b** could also be formed even though they present less exothermic reaction energies), they are in good agreement with the experimental findings.

The reactivities found for the free cage and its endohedral derivative can be described in terms of C–C bond distances, pyramidalization angles, and shapes of the lowest-lying unoccupied molecular orbitals. The most favorable addition sites present short C–C bond distances, that is indeed the case for bonds **1**, **7**, and **b** for D_{3h}-C_{78} (see Table 4.1). Similarly, bond **2** presents the longest C–C bond distance and gives a significantly endothermic reaction energy. However, there are some bonds that present similar bond distances and their reaction energies are exothermic (for example bond **c**). The most reactive bond in the case of $Sc_3N@D_{3h}$-C_{78} does also present the shortest C–C bond distance, but for instance bond **7** has the same C–C distance and its reaction energy is approximately 5 kcal·mol^{-1} less exothermic.

Table 4.1 Bond distances R_{CC} (Å) and pyramidalization angles θ_p (degrees)[a] for the bond-types in free and endohedral fullerene[b]

			C_{78}		$Sc_3N@C_{78}$	
Product	Bond-type		R_{CC}	θ_p[a]	R_{CC}	θ_p[a]
1	*A*	*[6,6]*	**1.369**	10.46	1.440	**13.80**
2	*C*	*[6,6]*	1.465	8.58	1.466	8.33
3	*B*	*[6,6]*	1.432	9.62	1.450	9.26
4	*B*	*[6,6]*	1.415	9.60	**1.426**	9.44
5	*B*	*[6,6]*	1.418	9.53	1.432	8.97
6	*B*	*[6,6]*	1.420	9.44	**1.400**	9.99
7	*A*	*[6,6]*	**1.388**	**11.64**	**1.400**	**11.21**
a	*D*	*[5,6]*	1.438	**11.64**	1.437	**11.21**
b	*D*	*[5,6]*	**1.410**	10.49	1.446	9.73
c	*D*	*[5,6]*	1.465	10.32	**1.423**	9.27
d	*D*	*[5,6]*	1.446	10.56	1.452	**12.00**
e	*D*	*[5,6]*	1.438	10.38	1.449	10.92
f	*D*	*[5,6]*	1.442	**11.13**	1.432	10.88

[a] Pyramidalization angles averaged over both atoms that constitute the bond under consideration
[b] In **boldface** the bonds that are predicted to be most reactive

In the case of the endohedral compound, the longest bond (**2**) does not possess the least favorable reaction energy. Hence, there is not an overall correlation between C–C bond distances and reaction energies, apart from the fact that the most reactive bonds do exhibit short C–C bond distances.

As it happens with bond distances, the prediction of the fullerene reactivity in terms of the pyramidalization angles is not straightforward. The most reactive sites exhibit from moderately to high values, however a large pyramidalization angle does not always correspond to an enhanced reactivity of the bond (see Table 4.1). The encapsulation of the Sc_3N moiety inside the cage leads to an increase of the pyramidalization angles, especially for those bonds situated close to the scandium influence. For instance, bond **1** in $Sc_3N@D_{3h}$-C_{78} presents the highest pyramidalization angle (13.8°), but the cycloaddition reaction over it is endothermic by 4 kcal·mol^{-1}. Therefore, the use of pyramidalization angles to predict fullerene reactivity does not always lead to the correct answer.

Finally, the cycloaddition reaction between 1,3-cis-butadiene and the fullerene compounds might also be understood in terms of the molecular orbitals of both reacting species. The most prominent interaction occurs between the HOMO of the diene and the LUMO of the fullerene, therefore those bonds presenting suitable shaped orbitals to interact with the HOMO of the diene might be the most favorable addition sites. In C_{78}, bonds **1**, **7** and **b** present suitable orbitals to interact, and are indeed the most reactive sites of the fullerene compound (see Fig. 4.3). However, several bonds present similar suitable antibonding orbitals to react with diene **1**, **2**, **3**, **4**, **6**, **7**, **c**, and **e** in the case of $Sc_3N@C_{78}$ (see Fig. 4.4). Among all bonds with suitable orbitals to interact only **6**, **4**, **7** and **c** present favorable reaction and activation energies. Moreover bond **d** does not possess suitable shaped orbitals and its reaction and activation barriers are substantially favorable. Hence, the

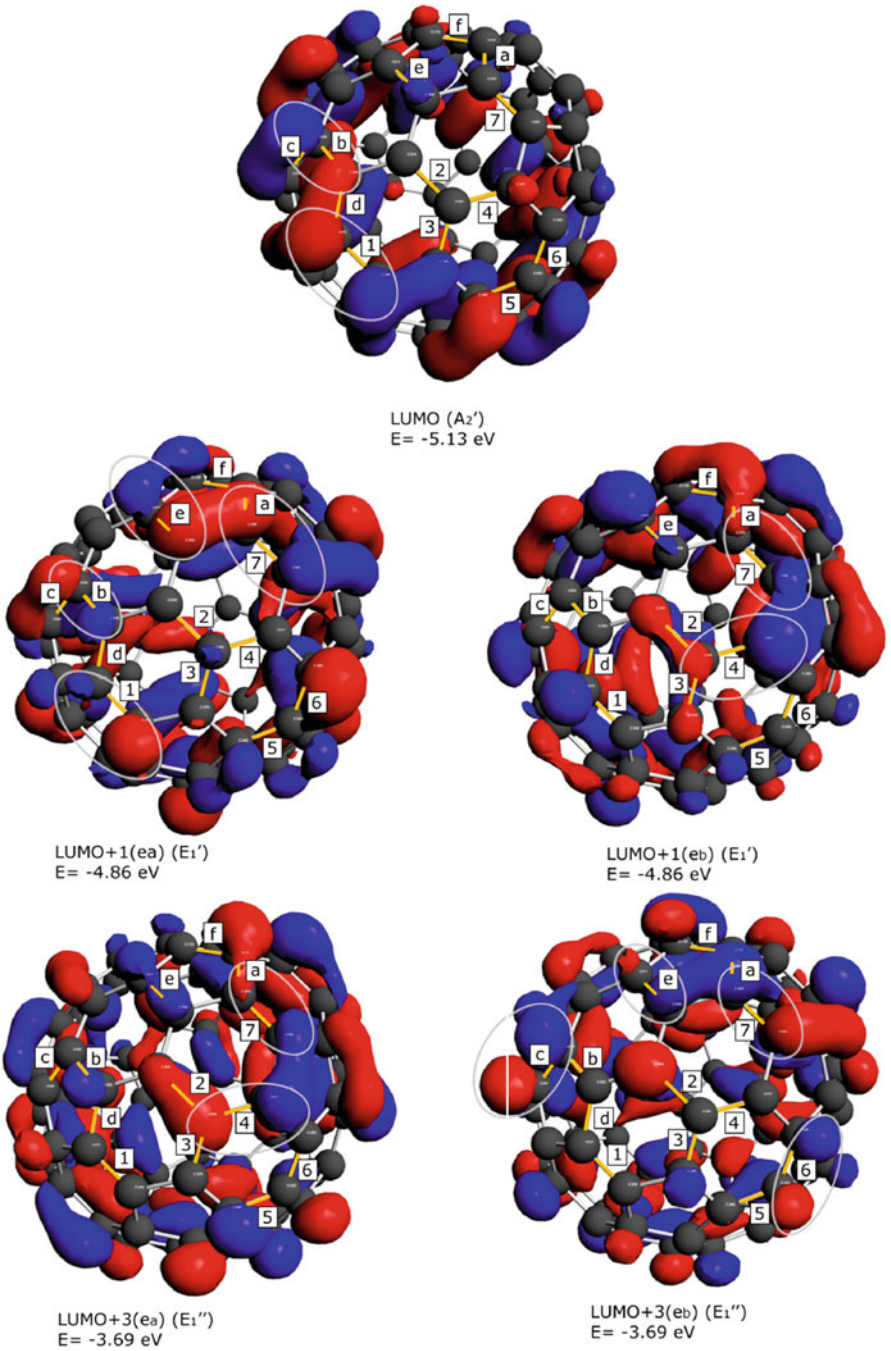

Fig. 4.3 Representation of the C_{78} LUMO and degenerate LUMO + 1 and LUMO + 3 molecular orbitals (isosurface value 0.02 a.u) where all non-equivalent [6,6] and [5,6] bonds have been marked. Those bonds with favorable orbitals to interact with the HOMO of the diene are marked with ellipses

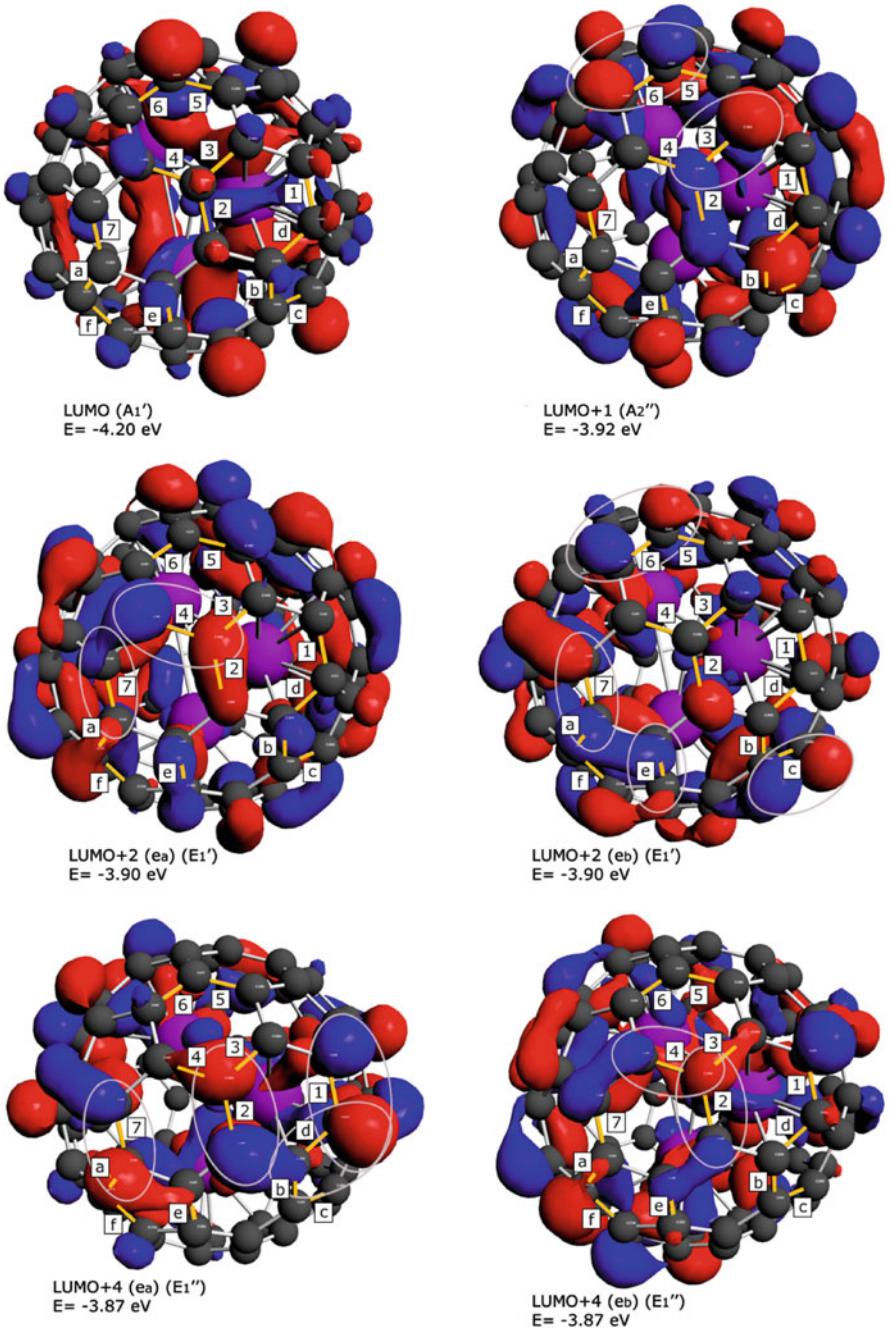

Fig. 4.4 Representation of the $Sc_3N@C_{78}$ LUMO, LUMO + 1, and degenerate LUMO + 2 and LUMO + 4 molecular orbitals (isosurface value 0.02 a.u.) where all non-equivalent [6,6] and [5,6] bonds have been marked. Those bonds with favorable orbitals to interact with the HOMO of the diene are marked with ellipses

predictions of reactivity for fullerene compounds using the LUMO orbitals are too imprecise, as one finds many bonds suitable to interact.

Although the previously mentioned descriptors do not give accurate results for describing the exohedral reactivity of the cages, the combination of all three descriptors (*C–C bond distances, pyramidalization angles and molecular orbital analysis*) gives quite successful results. Only bonds **1**, **7** and **b** in the case of C_{78}, and bonds **4**, **6**, **7**, and **c** in $Sc_3N@C_{78}$ fulfill the three criteria. They exhibit short C–C bond distances, relatively high pyramidalization angles and suitable orbitals to interact with diene. And in fact, our thermodynamic and kinetic study indeed shows these bonds to be most reactive.

4.3 The Diels-Alder Reaction on Endohedral $Y_3N@C_{78}$: The Importance of the Fullerene Strain Energy

In some experimental studies, it was observed that the exohedral reactivity of the TNT endohedral metallofullerenes is highly affected by the nature of the encapsulated cluster (Cardona et al. 2005a). Our initial study involving the Diels-Alder reaction on the endohedral scandium based fullerene compound has been extended to directly compare how the reactivity is affected by encapsulating either scandium or yttrium inside the cage (Osuna et al. 2009a). In the first part of this section, the preferred addition sites for the $Y_3N@D_{3h}$-C_{78} molecule will be thoroughly described as well as compared to the previously reported $Sc_3N@D_{3h}$-C_{78} and D_{3h}-C_{78} (Osuna et al. 2008). Finally, an insight into the exohedral reactivity of the most favorable isomer for the encapsulation of the large Y_3N unit is presented.

The large yttrium based TNT cluster is forced to adopt a pyramidal configuration inside the D_{3h}-C_{78} cage, and two clearly differentiated areas are present (see Fig. 4.5): the so-called *up* region, which is more influenced by the nitrogen atom, and the *down* part which has the yttrium atoms in close contact. In every region, 13 non equivalent bonds might be considered to take into account all possible addition sites: two type A [6,6] bonds (**1** and **7**), four type B [6,6] bonds (**3**, **4**, **5**, **6**), one type C [6,6] bond (**2**), and 6 type D [5,6] bonds (**a**-**f**). Our study of the Diels-Alder reaction at the ZORA-BP86/TZP//ZORA-BP86/DZP level on both faces of the fullerene indicates that both areas are equally reactive with energy differences of at most 1.6 kcal·mol^{-1}. The most stable regioisomer for the Diels-Alder cycloaddition reaction over the endohedral compound $Y_3N@D_{3h}$–C_{78} is shown to be favored over the [5,6] bond **d** that exhibits the longest bond distance in the initial fullerene ($\Delta E_R = -15.0$ kcal·mol^{-1}, $\Delta E^{\ddagger} = 17.1$ kcal·mol^{-1}). As far as we know, this is the first case of a cycloaddition reaction where the most stable addition is obtained over one of the longest C–C bonds in the cage. This observation is of significance as those bonds with the shortest bond distances are usually related with the most reactive positions. Therefore, bond distances cannot be considered a predictor of fullerene reactivity anymore, and as a consequence those studies

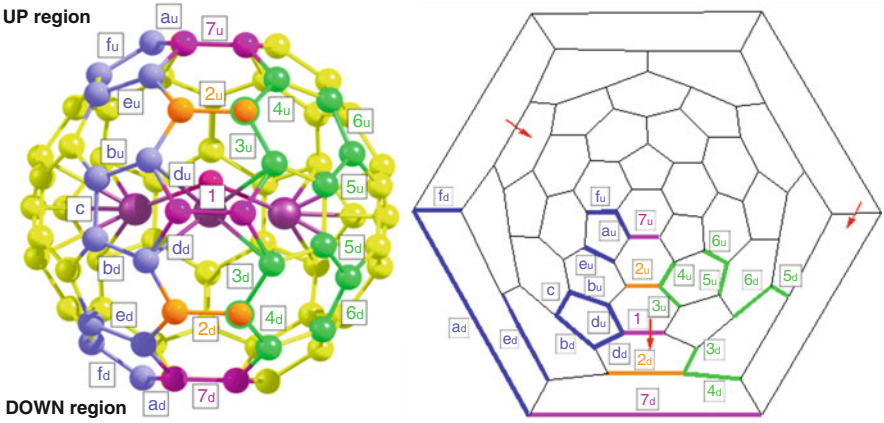

Fig. 4.5 Representation of all non-equivalents bonds of the $Y_3N@D_{3h}$-C_{78}. The Schlegel diagram of the fullerene (2D representation) is also depicted where the non-equivalent bonds are marked. The Y_3N cluster presents a pyramidal configuration and therefore two clearly differentiated areas exist. The up region is more affected by the nitrogen atom, whereas the *down* area is more influenced by the yttrium atoms

where only short bonds were investigated might not give the correct picture of the reactivity of endohedral fullerene compounds.

The second most favorable regioisomer corresponds to the addition over a type B [6,6] bond called **6** ($\Delta E_R = -11.0$ kcal·mol^{-1}, $\Delta E^{\ddagger} = 18.3$ kcal·mol^{-1}). Finally, although the reaction energy for the cycloaddition reaction to the [5,6] bond called **e** is hardly exothermic (-4.1 kcal·mol^{-1}), it does present a low activation barrier (17.2 kcal·mol^{-1}). Moreover, there is a difference of 4.1 kcal·mol^{-1} between the activation barrier of bond **e** situated in the *down* and *up* areas. The enhanced reactivity of bond **e** situated in the down region is basically attributed to the presence of suitable shaped orbitals to interact with diene at lower energy. Moreover, the cycloaddition reaction over bond $\mathbf{e_u}$ (i.e. situated in the up region) is disfavored as it breaks an attractive interaction between the N atom and this $\mathbf{e_u}$ bond.

By comparing the same Diels-Alder reaction over the related compounds D_{3h}-C_{78}, $Sc_3N@D_{3h}$-C_{78}, and $Y_3N@D_{3h}$-C_{78} different reactivity patterns are observed (see Fig. 4.6). For the free cage, the reaction is favored over the [5,6] bond called **b**. The second and third most stable regiosiomers correspond to the addition to the pyracylenic [6,6] bonds called **7** and **1**, respectively. Once the scandium based TNT cluster is encapsulated inside, the addition is basically preferred to the type B [6,6] bond called **6**. The other favorable interactions are over the type B [6,6] bond **4** and the type D [5,6] **c**. It should be emphasized here, that the most reactive bonds in $Sc_3N@D_{3h}$-C_{78} exhibit short C–C bond distances, relatively high pyramidalization angles and are situated far away from the scandium influence. In contrast to $Sc_3N@D_{3h}$-C_{78}, the reaction in the case of $Y_3N@D_{3h}$-C_{78} is basically favored over bond **d** having one of the yttrium atoms in close contact. This preference for reacting with a bond situated close to the yttrium atoms is due to two different factors. First, the D_{3h} cage is extremely deformed, especially in the

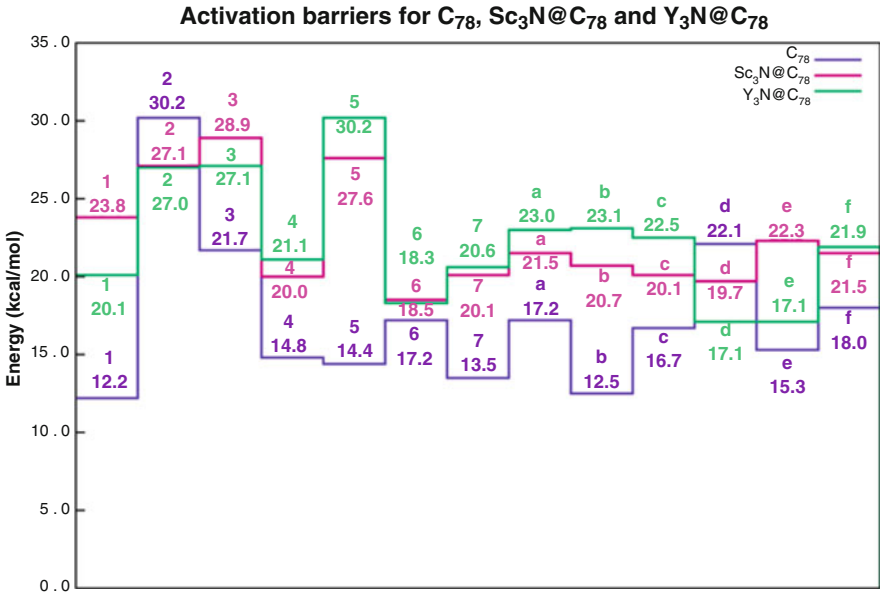

Fig. 4.6 The activation barriers in kcal·mol^{-1} obtained for D_{3h}-C_{78} (*represented in lilac*), $Sc_3N@D_{3h}$-C_{78} (*in pink*) and $Y_3N@D_{3h}$-C_{78} (*in green*)

pyracylenic areas situated close to the yttrium atoms which contain the most reactive bonds, thus the attack reduces the strain energy of the cage. Second, in the final adduct the Y_3N cluster gets additional space to adopt a more planar configuration. The C–C bond of the attacked bond **d** is practically broken and an open fulleroid is obtained. The addition to bond **d** is preferred as the diene has to be deformed to a lesser extent to react (*in the case of bonds **1** and **3** situated close to the yttrium atoms, the deformation of the diene is approximately 22 kcal·mol^{-1}, whereas only 14 in the case of **d***).

As observed in the previous section, the encapsulation of Sc_3N inside the D_{3h} cage produces a decrease of the exohedral reactivity. It is basically governed by the electronic charge transfer from the TNT to the fullerene that leads to LUMOs higher in energy. Most of the considered bonds in the case of $Y_3N@D_{3h}$-C_{78} slightly decrease their reactivity, which is consistent with the relatively larger HOMO-LUMO gap found for $Y_3N@D_{3h}$-C_{78} (1.26 and 1.22 eV for the yttrium and scandium based metallofullerenes, respectively) and the higher electron transfer produced in the case of yttrium.

4.4 The Diels-Alder Reaction on the C_2: 22010 Cage

The most favorable C_{78} cage to encapsulate the large Y_3N cluster is the non-IPR C_2: **22010** isomer where the TNT moiety can adopt a planar configuration (Popov and Dunsch 2007). The difference in energy between $Y_3N@D_{3h}$-C_{78} and $Y_3N@C_2$-C_{78}

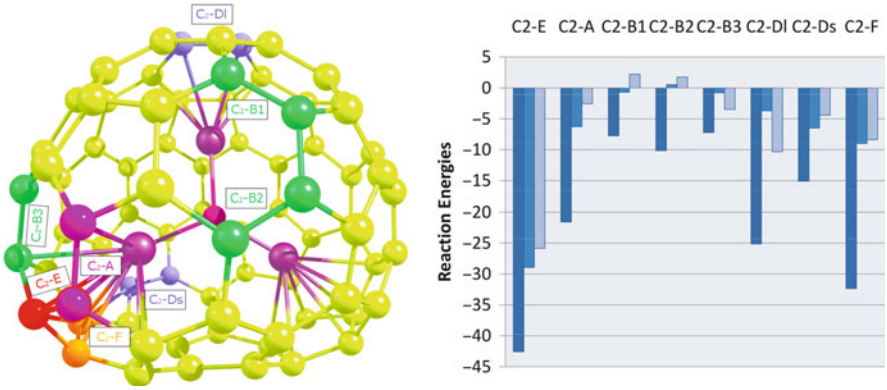

Fig. 4.7 Representation of the selected bonds of the $Y_3N@C_2$-C_{78} compound. The reaction energies obtained for the different cases studied: C_2-C_{78} (*represented in dark blue*), $Sc_3N@C_2$-C_{78} (*in blue*), and $Y_3N@C_2$-C_{78} (*in light blue*) are expressed in kcal·mol^{-1}. Different colors are used to indicate the different bond types studied: *pink*, [6,6] type A; *green*, [6,6] type B; *blue*, [5,6] type D; *red*, [5,5] type E; *orange*, [5,6] type F

is 20.2 kcal·mol^{-1} at ZORA-BP86/TZP//ZORA-BP86/DZP. The latter is similar to the difference of 21.1 kcal·mol^{-1} between the two synthesized and exohedrally functionalized D_{5h} and I_h cages of the C_{80} fullerene, which are both experimentally attainable (Popov and Dunsch 2007). Among all non-equivalent bonds of the C_2: **22010** cage, eight bonds were selected on the basis of the reactivity trends observed in the D_{3h} cage: one type E [5,5] bond only present in the non-IPR cages (called **C_2-E**), one type F [5,6] bond (**C_2-F**), two type B [6,6] bonds with short bond distances and situated far away from the metals (**C_2-B1**, **C_2-B2**), another type B [6,6] bond situated near one of the yttrium atoms (**C_2-B3**), one type D [5,6] bond with large C–C bond distances and positioned close to the yttrium metal (**C_2-Dl**), another type D [5,6] bond with short bond distance and situated far away from the yttrium influence (**C_2-Ds**), and finally one pyracylene [6,6] bond called **C_2-A** close to the yttrium atom (see Fig. 4.7).

Interestingly, the Diels-Alder reaction on $Y_3N@C_2$-C_{78} is favored over the [5,5] bond called **C_2-E** which has one of the yttrium atoms directly coordinated towards it. As far as we know, the reactivity of these [5,5] bonds was never assessed before. Although Campanera and coworkers predicted a low reactivity of these non-IPR bonds on the basis of the Mayer Bond Order analysis (Campanera et al. 2006), our theoretical findings indicate that the reaction is substantially exothermic (−25.9 kcal·mol^{-1}) and highly stereoselective. The reaction over the rest of the considered bonds is from 15.6 to 28.1 kcal·mol^{-1} less favorable. This observed tendency to react with those bonds situated close to the metal atoms might either be influenced by the presence of the yttrium atoms or be dictated by the C_2 cage. Hence, the Diels-Alder reaction was also assessed in the case of the free C_2 and the scandium based endohedral derivative. Interestingly, the reaction is found to be favored over the same [5,5] bond called **C_2-E** in both C_2-C_{78} and $Sc_3N@C_2$-C_{78} compounds (the reaction energies obtained are −42.6 and −28.9 kcal·mol^{-1}, respectively).

Therefore, our theoretical calculations indicate that the exohedral functionalization of synthesized $Tm_3N@C_{78}$ (Krause et al. 2005), $Dy_3N@C_{78}$ (Popov et al. 2007) and $Gd_3N@C_{78}$ (Beavers et al. 2009) might be stereoselectively produced over the [5,5] bonds.

4.5 Reactivity and Regioselectivity of Noble Gas Endohedral Fullerenes Ng@C_{60} and $Ng_2@C_{60}$ (Ng = He-Xe)

Krapp and Frenking performed a theoretical study on the noble gas dimers endohedral fullerenes $Ng_2@C_{60}$ (Ng = He-Xe) (Krapp and Frenking 2007). Interestingly, they observed that an electron transfer of 1–2 electrons is produced in the case of the larger noble gas homologues, in particular for the Xe_2 dimer. Free noble gas dimers are rarely observed, however a genuine chemical bond is formed once the Xe_2 unit is trapped inside the fullerene moiety. In addition to that, the encapsulation of Ar_2, Kr_2 and Xe_2 was found to affect the C–C bond distances of the C_{60} compound as well as the pyramidalization angles. Therefore, a change on the exohedral reactivity might be observed. In this section, the Diels-Alder reaction is discussed either for the single noble gas endohedral compounds Ng@C_{60} (Ng = He-Xe) and the noble gas dimers endohedral fullerenes $Ng_2@C_{60}$ at the ZORA-BP86/TZP level of theory (Osuna et al. 2009b).

First, the Diels-Alder reaction between 1,3-cis-butadiene and C_{60} has been studied as reference. The reaction is favored over the pyracylene [6,6] bond that presents a reaction energy of -20.7 kcal·mol^{-1} and an activation barrier of 12.7 kcal·mol^{-1}. The [5,6] bonds are substantially less reactive as the reaction and activation energies obtained are 15.4 and 8.3 kcal·mol^{-1} less favorable. The noble gas encapsulation hardly affects the exohedral reactivity of the cage, i.e. differences of less than 0.4 kcal·mol^{-1} were observed for both the reaction energies and barriers.

More interesting results were obtained for the case of the noble gas dimer encapsulation. Krapp and Frenking studied the cage isomerism of the noble gas endohedral derivatives and observed that the most stable structure was the D_{3d} isomer for He-Kr, and the D_{5d} isomer for Xe (Krapp and Frenking 2007). However, the energy differences between the different isomers were found to be very low. Therefore, we decided to study the Diels-Alder reaction on the D_{5d} isomer for all noble gases for many reasons. First, the comparison of the different bonds can only be done considering the same isomer for all cases studied. Second, the most interesting compound to study is the xenon-based endohedral fullerene because of the electron transfer produced. Finally, the energies for the encapsulation of the He-Kr atoms inside the D_{5d} isomer differed by less than 2 kcal·mol^{-1} from the D_{3d} equivalents. Note that for the D_{5d} isomer there are six non-equivalent type D [5,6] bonds (called **a**, **b**, **c**, **d**, **e**, and **f**) and three type A [6,6] bonds (called **1**, **2**, and **3**) (see Fig. 4.8).

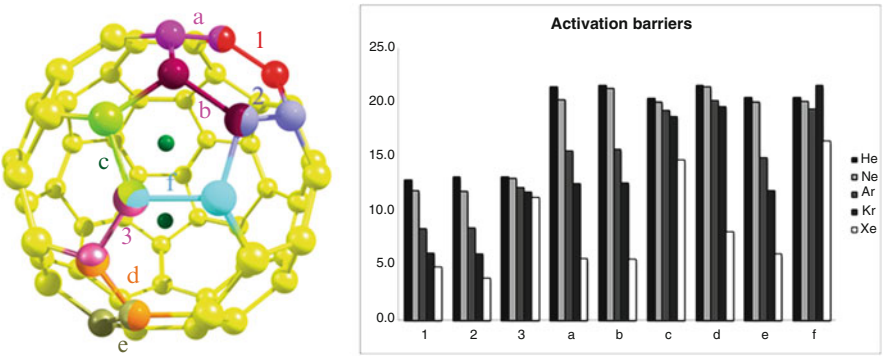

Fig. 4.8 Representation of all non-equivalent bonds of the $Ng_2@C_{60}$ compound. The activation energies (in kcal·mol^{-1}) corresponding to the Diels-Alder cycloaddition reaction between 1,3-butadiene and all non-equivalent bonds for all considered noble gas endohedral compounds. $Ng_2@C_{60}$ has been represented on the *right*. A grey scale has been used to represent the different noble gases endohedral compounds: *black color* is used to represent the helium-based fullerene, *light grey* for neon, *medium grey* for argon, *dark grey* for krypton, and *white* for xenon

The Diels-Alder reaction produced on the lighter noble gas dimer compounds (i.e. $He_2@C_{60}$ and $Ne_2@C_{60}$) presents reaction and activation barriers that are close to the ones obtained for free C_{60}. I.e., the reaction energies for the most reactive bond **1** are compared to the free fullerene 0.2 and 2.4 kcal·mol^{-1} more favorable for the helium and neon dimer compounds, respectively. Likewise, the activation barrier for the addition to bond **1** is 12.8 and 11.9 kcal·mol^{-1} for the $He_2@C_{60}$ and $Ne_2@C_{60}$ cases, respectively. The other [6,6] bonds present similar reaction and activation energies, whereas [5,6] bonds are much more less reactive. It is important to remark that the addition of 1,3-butadiene produces a rotation of the noble gas dimer which is reoriented during the course of the reaction from the initial position to face the attacked bond.

Once Ar_2 and Kr_2 are inserted inside C_{60}, the reaction becomes substantially more exothermic (−32.2 and −39.9 kcal·mol^{-1} for bonds **1** and **2**, respectively), and the activation barriers are largely reduced (to ca. 8 and 6 kcal·mol^{-1} for the Ar_2 and Kr_2 compounds, respectively). The addition to the [6,6] bond **3** is less favored, as the noble gas moiety is not totally reoriented to face the attacked bond. Of course, the larger the noble gas atom, the more impeded the rotation of the noble gas dimer inside the cage. Hence, for the larger noble gas endohedral compounds the addition is favored over those bonds situated close to the C_5 axis where the dimer is initially contained. This lack of rotation leads to substantially less favored reaction and activation barriers.

The preferred addition site for the Xe-based compound corresponds to [6,6] bond **1** (−44.9 kcal·mol^{-1}), however the [5,6] bonds **a**, **b** and **e** do also present favorable reaction energies (−44.6,−44.5, and−45.5 kcal·mol^{-1}, respectively). On the other hand, the lowest activation energy is found for the [6,6] bond **2** (3.8 kcal·mol^{-1}), nonetheless bonds **1**, **a**, **b**, and **e** also present low energy barriers (4.9, 5.7, 5.6, 6.1 kcal·mol^{-1}, respectively). Therefore, the reaction is no longer

regioselective as five (!) regioisomers might be formed during the reaction between 1,3-butadiene and $Xe_2@C_{60}$.

The enhanced reactivity along the series $He_2@C_{60} < Ne_2@C_{60} < Ar_2@C_{60} < Kr_2@C_{60} < Xe_2@C_{60}$ can be attributed to several factors. First, the HOMO-LUMO gap is reduced from 1.63 eV for $He_2@C_{60}$ to 0.75 eV for $Xe_2@C_{60}$ (for the free cage it is 1.66 eV), which is basically produced by a slight stabilization of the LUMO and a major destabilization of the HOMO. The latter is a complex situation as the HOMO for the lighter noble gas compounds (a_{1u} orbital, for He-Ar) is different to that of xenon and krypton fullerenes (a_{2u} orbital that primarily presents antibonding σ* orbitals in the noble gas dimer unit). The destabilization of the a_{2u} orbital increases from He to Xe because of the reduction of the Ng-Ng distance along the series. Second, the deformation energy of the cage also plays an important role. The encapsulation of He_2 and Ne_2 inside C_{60} hardly affects the cage as the calculated deformation energies are 0 and less than 1 kcal·mol^{-1}, respectively. However, the insertion of the larger Ar_2, Kr_2, and Xe_2 leads to a deformation energy of 11.2, 22.5 and 34.1 kcal·mol^{-1}, respectively. The high deformation energy found, especially for the xenon-based compound, leads to a highly strained cage where all [5,6] and [6,6] bonds situated close to the initial position of the Xe_2 dimer are equally reactive. The reaction is then extremely exothermic and unselective as the strain of the cage is partially released after reaction. Finally, the Ng–Ng bond distance elongation does also contribute to the enhanced reactivity for the heavier noble gas compounds. After reaction, the Ng-Ng distance is increased by 0.028, 0.043, 0.040, 0.035, and 0.054 Å along the $He_2-Xe_2@C_{60}$ series which corresponds to an stabilization of −0.2, −1.0, −4.1, −5.3, and −10.4 kcal·mol^{-1}. This decompression represents an important contribution to the exothermicity of the reaction for those bonds where the Ng dimer is reoriented facing the attacked bond.

4.6 Conclusions

The effect of the encapsulation of trimetallic nitride (TNT) complexes or noble gas dimers on the exohedral reactivity of fullerene cages is profound. Not only does the encapsulation affect the reactivity, it also changes the regioselectivity patterns. For the TNT complexes, a reduction in the reactivity is observed corresponding to an increase of the barriers by some 6 kcal·mol^{-1}, and a decrease of the reaction energy by some 12–20 kcal·mol^{-1}. The preferred addition sites for the free C_{78} fullerene are totally different from those for $Sc_3N@C_{78}$, which are again radically different for $Y_3N@C_{78}$. Both the free and $Sc_3N@C_{78}$ fullerenes prefer to react over C–C bonds with short distances, which in the case of $Sc_3N@C_{78}$ are located far away from (the influence of) the scandium atoms. In contrast, the $Y_3N@C_{78}$ fullerene preferably reacts over long C–C bonds, close to the yttrium atoms. This latter is in part attributed to the deformation of the cage.

The deformation of the cage also plays a role for the encapsulation of noble gas dimers in C_{60}, but there it leads to drastically more reactive compounds. I.e. the

larger the noble-gas atoms, the smaller the reaction barrier and the more exothermic are the products. Similar to $Y_3N@C_{78}$ this results primarily from a strained fullerene, which is (partially) released upon reaction. Also the decompression of the noble gas dimer contributes, as is the major destabilization of the HOMO orbital. For the xenon-dimer fullerene, which is characterized by a charge transfer of one to two electrons to the fullerene, many reactive bonds are found and there is almost no regioselectivity anymore.

Acknowledgments The following organizations are thanked for financial support: the Ministerio de Ciencia e Innovación (MICINN, project numbers CTQ2008-03077/BQU and CTQ2008-06532/BQU), and the DIUE of the Generalitat de Catalunya (project numbers 2009SGR637 and 2009SGR528). Excellent service by the Centre de Supercomputació de Catalunya (CESCA) is gratefully acknowledged. The authors also are grateful to the computer resources, technical expertise, and assistance provided by the Barcelona Supercomputing Center – Centro Nacional de Supercomputación (BSC-CNS, MareNostrum). Support for the research of M. Solà was received through the ICREA Academia 2009 prize for excellence in research funded by the DIUE of the Generalitat de Catalunya.

Appendix: Computational Details

All Density Functional Theory (DFT) calculations were performed with the Amsterdam Density Functional (ADF) program (Baerends et al. 2009; te Velde et al. 2001) and the related QUILD (QUantum-regions Interconnected by Local Descriptions) (Swart and Bickelhaupt 2008). The molecular orbitals (MOs) were expanded in an uncontracted set of Slater type orbitals (STOs) of triple-ζ (TZP) quality containing diffuse functions and one set of polarization functions. Core electrons (1s for 2nd period, 1s2s2p for 3rd-4th period) were not treated explicitly during the geometry optimizations (frozen core approximation) (te Velde et al. 2001), as it was shown to have a negligible effect on the obtained geometries (Swart and Snijders 2003). An auxiliary set of s, p, d, f, and g STOs was used to fit the molecular density and to represent the Coulomb and exchange potentials accurately for each SCF cycle. Energies and gradients were calculated using the local density approximation (Slater exchange and VWN correlation) (Vosko et al. 1980) with non-local corrections for exchange (Becke 1988) and correlation (Perdew 1986) included self-consistently (i.e. the BP86 functional). For the studies with heavier elements, relativistic corrections were included self-consistently using the Zeroth Order Regular Approach (ZORA) (van Lenthe et al. 1993; te Velde et al. 2001).

The actual geometry optimizations and transition state searches were performed with the QUILD program (Swart and Bickelhaupt 2008). QUILD constructs all input files for ADF, runs ADF, and collects all data; ADF is used only for the generation of the energy and gradients. Furthermore, the QUILD program uses improved geometry optimization techniques, such as adapted delocalized coordinates (Swart and Bickelhaupt 2006) and specially constructed model Hessians with the appropriate number of eigenvalues (Swart and Bickelhaupt 2006, 2008). The latter is of

particular use for TS searches. All TSs have been characterized by computing the analytical vibrational frequencies, to have one (and only one) imaginary frequency corresponding to the approach of the reacting molecules.

References

Agnoli AL, Jungmann D, Lochner B (1987) Neurosurg Rev 10:25–29
Aihara J-i (2001) Chem Phys Lett 343:465–469
Akasaka T, Nagase S (2002) Endofullerenes: a new family of carbon clusters. Kluwer Academic, Dordrecht
Baerends EJ, Autschbach J, Bashford D, Berger JA, Bérces A, Bickelhaupt FM, Bo C, de Boeij PL, Boerrigter PM, Cavallo L, Chong DP, Deng L, Dickson RM, Ellis DE, van Faassen M, Fan L, Fischer TH, Fonseca Guerra C, Giammona A, Ghysels A, van Gisbergen SJA, Götz AW, Groeneveld JA, Gritsenko OV, Grüning M, Harris FE, van den Hoek P, Jacob CR, Jacobsen H, Jensen L, Kadantsev ES, van Kessel G, Klooster R, Kootstra F, Krykunov MV, van Lenthe E, Louwen JN, McCormack DA, Michalak A, Mitoraj M, Neugebauer J, Nicu VP, Noodleman L, Osinga VP, Patchkovskii S, Philipsen PHT, Post D, Pye CC, Ravenek W, Rodríguez JI, Romaniello P, Ros P, Schipper PRT, Schreckenbach G, Seth M, Snijders JG, Solà M, Swart M, Swerhone D, te Velde G, Vernooijs P, Versluis L, Visscher L, Visser O, Wang F, Wesolowski T.A, van Wezenbeek EM, Wiesenekker G, Wolff SK, Woo TK, Yakovlev AL, Ziegler T (2009) ADF 2009.01. SCM, Amsterdam
Beavers CM, Chaur MN, Olmstead MM, Echegoyen L, Balch AL (2009) J Am Chem Soc 131:11519–11524
Becke AD (1988) Phys Rev A 38:3098–3100
Cai T, Ge ZX, Iezzi EB, Glass TE, Harich K, Gibson HW, Dorn HC (2005) Chem Commun 3594–3596
Cai T, Xu L, Anderson MR, Ge Z, Zuo T, Wang X, Olmstead MM, Balch AL, Gibson HW, Dorn HC (2006) J Am Chem Soc 128:8581–8589
Cai T, Xu L, Gibson HW, Dorn HC, Chancellor CJ, Olmstead MM, Balch AL (2007) J Am Chem Soc 129:10795–10800
Cai T, Xu L, Shu C, Champion HA, Reid JE, Anklin C, Anderson MR, Gibson HW, Dorn HC (2008) J Am Chem Soc 130:2136–2137
Campanera JM, Bo C, Olmstead MM, Balch AL, Poblet JM (2002) J Phys Chem A 106:12356–12364
Campanera JM, Bo C, Poblet JM (2005) Angew Chem Int Ed 44:7230–7233
Campanera JM, Bo C, Poblet JM (2006) J Org Chem 71:46–54
Cao B, Nikawa H, Nakahodo T, Tsuchiya T, Maeda Y, Akasaka T, Sawa H, Slanina Z, Mizorogi N, Nagase S (2008) J Am Chem Soc 130:983–989
Cardona CM, Kitaygorodskiy A, Echegoyen L (2005a) J Am Chem Soc 127:10448–10453
Cardona CM, Kitaygorodskiy A, Ortiz A, Herranz MA, Echegoyen L (2005b) J Org Chem 70:5092–5097
Cardona CM, Elliott B, Echegoyen L (2006) J Am Chem Soc 128:6480–6485
Chai Y, Guo T, Jin C, Haufler RE, Chibante LPF, Fure J, Wang L, Alford JM, Smalley RE (1991) J Phys Chem 95:7564–7568
Chaur MN, Melin F, Athans AJ, Elliott B, Walker BC, Holloway K, Echegoyen L (2008) Chem Commun 2665
Chaur MN, Melin F, Ortiz AL, Echegoyen L (2009) Angew Chem Int Ed 48:7514–7538
Chen N, Fan LZ, Tan K, Wu YQ, Shu CY, Lu X, Wang C-R (2007a) J Phys Chem C 111:11823–11828
Chen N, Zhang E-Y, Tan K, Wang C-R, Lu X (2007b) Org Lett 9:2011–2013

Diener MD, Alford JM, Kennel SJ, Mirzadeh S (2007) J Am Chem Soc 129:5131–5138
Dunsch L, Yang S (2007) Small 3:1298–1320
Echegoyen L, Chancellor CJ, Cardona CM, Elliott B, Rivera J, Olmstead MM, Balch AL (2006) Chem Commun 2653–2655
Guha S, Nakamoto K (2005) Coord Chem Rev 249:1111–1132
Guldi DM, Feng L, Radhakrishnan SG, Nikawa H, Yamada M, Mizorogi N, Tsuchiya T, Akasaka T, Nagase S, Herranz MA, Martín N (2010) J Am Chem Soc 1332:9078–9086
Haddon RC (2001) J Phys Chem A 105:4164–4165
Haddon RC, Chow SY (1998) J Am Chem Soc 120:10494–10496
Harneit W (2002) Phys Rev A 65:032322
Heath JR, O'Brien SC, Zhang Q, Liu Y, Curl RF, Kroto HW, Tittel FK, Smalley RE (1985) J Am Chem Soc 107:7779–7780
Hu H, Cheng W-D, Huang S-H, Xie Z, Zhang H (2008) J Theor Comput Chem 7:737–749
Iiduka Y, Ikenaga O, Sakuraba A, Wakahara T, Tsuchiya T, Maeda Y, Nakahodo T, Akasaka T, Kako M, Mizorogi N, Nagase S (2005) J Am Chem Soc 127:9956–9957
Kobayashi K, Nagase S, Yoshida M, Osawa E (1997) J Am Chem Soc 119:12693–12694
Krapp A, Frenking G (2007) Chem Eur J 13:8256–8270
Krause M, Wong J, Dunsch L (2005) Chem Eur J 11:706–711
Kroto HW (1987) Nature 329:529–531
Kroto HW, Heath JR, O'Brien SC, Curl RF, Smalley RE (1985) Nature 318:162–163
Laus S, Sitharaman B, Tóth É, Bolskar RD, Helm L, Wilson LJ, Merbach AE (2007) J Phys Chem C 111:5633–5639
Lee HM, Olmstead MM, Iezzi E, Duchamp JC, Dorn HC, Balch AL (2002) J Am Chem Soc 124:3494–3495
Lu X, Nikawa H, Nakahodo T, Tsuchiya T, Ishitsuka MO, Maeda Y, Akasaka T, Toki M, Sawa H, Slanina Z, Mizorogi N, Nagase S (2008) J Am Chem Soc 130:9129–9136
Lu X, Nikawa H, Feng L, Tsuchiya T, Maeda Y, Akasaka T, Mizorogi N, Slanina Z, Nagase S (2009) J Am Chem Soc 131:12066–12067
Martín N (2006) Chem Commun 2093–2104
Mayer I (1983) Chem Phys Lett 97:270–274
Osuna S, Swart M, Campanera JM, Poblet JM, Solà M (2008) J Am Chem Soc 130:6206–6214
Osuna S, Swart M, Solà M (2009a) J Am Chem Soc 131:129–139
Osuna S, Swart M, Solà M (2009b) Chem Eur J 15:13111–13123
Parr RG, Chattaraj PK (1991) J Am Chem Soc 113:1854–1855
Pearson RG (1997) Chemical Hardness: applications from molecules to solids. Wiley-VCH, Oxford
Pearson RG (1999) J Chem Educ 76:267–275
Perdew JP (1986) Phys Rev B 33:8822–8824, Erratum: ibid. **34**, 7406–7406 (1986)
Pietzak B, Weidinger K-P, Dinse A, Hirsch A (2002) In: Akasaka T, Nagase S (eds) Endofullerenes: a new family of carbon clusters. Kluwer Academic, Amsterdam, pp 13–66
Popov AA, Dunsch L (2007) J Am Chem Soc 129:11835–11849
Popov AA, Dunsch L (2009) Chem Eur J 15:9707–9729
Popov AA, Krause M, Yang S, Wong J, Dunsch L (2007) J Phys Chem B 111:3363–3369
Rodríguez-Fortea A, Campanera JM, Cardona CM, Echegoyen L, Poblet JM (2006) Angew Chem Int Ed 45:8176–8180
Schmalz TG, Seitz WA, Klein DJ, Hite GE (1988) J Am Chem Soc 110:1113–1127
Shultz MD, Duchamp JC, Wilson JD, Shu C-Y, Ge J, Zhang J, Gibson HW, Fillmore HL, Hirsch JI, Dorn HC, Fatouros PP (2010) J Am Chem Soc 132:4980–4981
Stevenson S, Fowler PW, Heine T, Duchamp JC, Rice G, Glass T, Harich K, Hajdu E, Bible R, Dorn HC (2000) Nature 408:427–428
Stevenson S, Stephen RR, Amos TM, Cadorette VR, Reid JE, Phillips JP (2005) J Am Chem Soc 127:12776–12777
Swart M, Bickelhaupt FM (2006) Int J Quantum Chem 106:2536–2544

Swart M, Bickelhaupt FM (2008) J Comput Chem 29:724–734
Swart M, Snijders JG (2003) Theor Chem Acc 110:34–41, Erratum, (2004) Theor Chem Acc 111:56
te Velde G, Bickelhaupt FM, Baerends EJ, Fonseca Guerra C, van Gisbergen SJA, Snijders JG, Ziegler T (2001) J Comput Chem 22:931–967
Tellgmann R, Krawez N, Lin S-H, Hertel IV, Campbell EEB (1996) Nature 382:407–408
Thilgen C, Diederich F (2006) Chem Rev 106:5049–5135
Torrent-Sucarrat M, Luis JM, Duran M, Solà M (2001) J Am Chem Soc 123:7951–7952
Valencia R, Rodríguez-Fortea A, Poblet JM (2007) Chem Commun 4161–4163
Valencia R, Rodríguez-Fortea A, Clotet A, de Graaf C, Chaur MN, Echegoyen L, Poblet JM (2009) Chem Eur J 15:10997–11009
van Lenthe E, Baerends EJ, Snijders JG (1993) J Chem Phys 99:4597–4610
Vosko SH, Wilk L, Nusair M (1980) Can J Phys 58:1200–1211
Wang G-W, Saunders M, Cross RJ (2001) J Am Chem Soc 123:256–259
Whitehouse DB, Buckingham AD (1993) Chem Phys Lett 207:332–338
Yamada M, Okamura M, Sato S, Someya CI, Mizorogi N, Tsuchiya T, Akasaka T, Kato T, Nagase S (2009) Chem Eur J 15:10533–10542